

Structure and Dynamics of Ionic Liquids: Trimethylsilylpropyl-Substituted Cations and Bis(sulfonyl)amide Anions

Boning Wu,¹ Yuki Yamashita,² Takatsugu Endo,² Kenji Takahashi,^{2, a)} and Edward W. Castner Jr.^{1, a)}

¹⁾*Department of Chemistry and Chemical Biology, Rutgers, The State University of New Jersey, Piscataway, NJ 08854, United States*

²⁾*Institute of Science and Engineering, Kanazawa University, Kakuma-machi, Kanazawa, 920-1192, Japan*

Ionic liquids with cationic organosilicon groups have been shown to have a number of useful properties, including reduced viscosities relative to the homologous cations with hydrocarbon substituents on the cations. We report structural and dynamical properties of four ionic liquids having a trimethylsilylpropyl functional group, including 1-methyl-3-trimethylsilylpropylimidazolium (Si-C₃-mim⁺) cation paired with three anions: bis(fluorosulfonyl)imide (FSI⁻), bis(trifluoromethanesulfonyl)imide (NTf₂⁻) and bis(pentafluoroethanesulfonyl)imide (BETI⁻); as well as the analogous N-methyl-N-trimethylsilylpropylpyrrolidinium (Si-C₃-Pyr⁺) cation paired with NTf₂⁻. This choice of ionic liquids permits us to systematically study how increasing the size and hydrophobicity of the anions affects the structural and transport properties of the liquid. Structure factors for the ionic liquids were measured using high energy X-ray diffraction and calculated from molecular dynamics simulations. The liquid structure factors reveal first sharp diffraction peaks (FSDPs) for each of the four ionic liquids studied. Interestingly, the domain size for Si-C₃-mim⁺/NTf₂⁻ indicated by the maxima for these peaks is larger than for the more polar ionic liquid with a similar chain length, 1-pentamethyldisiloxymethyl-3-methyl-imidazolium bis(trifluoromethanesulfonyl)imide (SiOSi-mim⁺/NTf₂⁻). For the series of Si-C₃-mim⁺ ionic liquids, as the size of the anion increases, the position of FSDP indicates that the intermediate range order domains decrease in size, contrary to expectation. Diffusivities for the anions and cations are compared for a series of both hydrocarbon-substituted and silicon-substituted cations. All of the anions show the same scaling with temperature, size and viscosity, while the cations show two distinct trends—one for hydrocarbon-substituted cations and another for organosilicon-substituted cations, with the latter displaying decreased friction.

^{a)}Electronic mail: ktkenji@staff.kanazawa-u.ac.jp, ed.castner@rutgers.edu

I. INTRODUCTION

Ionic liquids (ILs) with silicon-containing cations (Si-ILs) were shown to have significantly reduced viscosities relative to the homologous species where the silicon atom is replaced by a carbon. Shirota and Castner showed that the viscosities could be 1.6 times lower for 1-trimethylsilylmethyl-3-methyl-imidazolium (Si-mim⁺) than for 1-methyl-3-neopentylimidazolium (C-mim⁺) cations paired with the NTf₂⁻ anion, with the ratio of viscosities increasing to a factor of 7.4 when BF₄⁻ is used as the anion.¹ This effect was further investigated by expanding the series of ILs to include pentamethyldisiloxy and silylphenyl groups,² and by studying the transport properties of the anions and cations using pulsed-gradient spin-echo (PG-SE) NMR³ and laser transient-grating methods.⁴ Low viscosities and high conductivities have also been reported for other Si-ILs.^{5,6} Applications using Si-ILs have been reported for gas separations,⁷ as polymer gel electrolytes for dye-sensitized solar cells,^{8,9} and as surfactant materials.¹⁰

The local structures and interactions in ionic liquids have been fully investigated by X-ray scattering, neutron scattering and molecular dynamics simulations in many studies.^{11–38} For NTf₂⁻-anion ILs, there is a sharp division between inter- and intra-molecular structure for the scattering vector value of $q=2 \text{ \AA}^{-1}$.³⁹ For the inter-molecular structure regime, there are three typical peaks in this region of the structure factor $S(q)$. The *adjacency peak*, with a maximum typically found at about $q \sim 1.4 \text{ \AA}^{-1}$, arises from the interactions of ions with their closest neighbors. The *charge-charge correlation peak* is usually centered near $q=0.8 \text{ \AA}^{-1}$, which reveals the interactions between ions and their second coordination shell. For those ILs with sufficiently large spatial extent, a *pre-peak* or *first sharp diffraction peak* (FSDP) appears at the lowest values of q , typically in the range from 0.2-0.6 \AA^{-1} .^{12,40,41} Most commonly, the FSDP results from intermediate range order arising from nano-domain segregation between non-polar alkyl tails on either the cations^{11,18,42–44} or anions^{45,46} that locally separate from the polar anionic and cationic head groups. Recently, we have reported that more polar groups such as a pentamethyldisiloxy tail can also lead to this kind of nano-phase segregation.⁴⁷ A third mechanism for such intermediate range order can arise from H-bonding networks in liquids such as ethyl- and propyl-ammonium nitrate.^{11,22,48,49}

Previously we reported the bulk liquid structure of three Si-ILs with NTf₂⁻ anion, 1-trimethylsilylmethyl-3-methyl-imidazolium (Si-mim⁺), 1-pentamethyldisiloxymethyl-3-

methyl-imidazolium (SiOSi-mim⁺) and 1-trimethylsilylmethyl-3-methyl-pyrroldinium (Si-pyrr⁺).⁴⁷ We also studied an IL with a hydrocarbon side chain cation (C-IL), 1-methyl-3-neopentylimidazolium bis(trifluoromethanesulfonyl)imide (C-mim⁺/NTf₂⁻), which differs from Si-mim⁺/NTf₂⁻ only by the replacement of the Si atom by C.⁴⁷ We obtained the structure factors for these ILs using high energy X-ray scattering and molecular dynamics simulation methods.⁴⁷

We found that the structure of Si-mim⁺/NTf₂⁻ is very similar to its carbon homolog C-mim⁺/NTf₂⁻. There are two notable differences between these two ILs. The first is that the adjacency peak shifts to lower values of q for Si-mim⁺/NTf₂⁻, which is caused by the larger volume of Si-mim⁺ cation. The second difference is that the charge-charge correlation peak in C-mim⁺/NTf₂⁻ is more sharply defined, which we believe is evidence for stronger interactions between ions in C-mim⁺/NTf₂⁻ than in Si-mim⁺/NTf₂⁻. This observation is consistent with the conclusion by Shirota *et al.* using femtosecond Kerr effect spectroscopy.

In this work, we discuss ILs with two different silicon-containing cations with longer $-(\text{CH}_2)_3\text{Si}(\text{CH}_3)_3$ tails, 1-methyl-3-trimethylsilylpropylimidazolium (Si-C₃-mim⁺) and N-methyl-N-trimethylsilylpropylpyrrolidinium (Si-C₃-Pyrr⁺). The molecular structure of cations and anions we studied are shown in Fig. 1. We note that both of these cations have a similar spatial extent to the SiOSi-mim⁺ cation, while the trimethylsilylpropyl group is less polar than the pentamethyldisiloxy group.

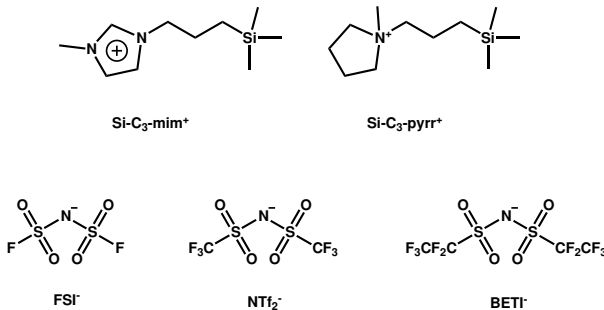


FIG. 1. The molecular structure of silicon ionic liquid cations and anions.

We are also interested in the effect of the anionic size and properties on the bulk structure of the ILs. In this study, we report structural details for the Si-C₃-mim⁺ cation paired with each of three sulfonylimide based anions: bis(fluorosulfonyl)imide (FSI⁻), bis(trifluoromethanesulfonyl)imide (NTf₂⁻) and bis(pentafluoroethanesulfonyl)imide (BETI⁻). There are

some studies focusing on the effect of anion type on structure of ILs,^{33,45,46,50,51} but there are fewer reports on the dependence of IL structure on anion size and anion chain length.

Unique features of the Si-ILs appear not only in the liquid structure factors and ionic interactions, but also in transport properties.¹⁻⁵ Recently, Endo *et al.* revealed that solute diffusion in Si-ILs, particularly for small sizes of diffusing molecules, is faster than for similar C-ILs when compared using the Stokes-Einstein plot, *i. e.*, normalizing by $T/(\eta \times r)$. This clearly indicates that solute diffusion mechanism differs in each medium, which we will show is likely to be the case for diffusion of the IL anions and cations themselves. In the last section of our results, anionic and cationic self-diffusion coefficients for Si-ILs were measured with PG-SE NMR and compared to those for C-ILs.

II. METHODS

Preparation of Ionic Liquids

The synthetic procedure for this set of Si-ILs was reported previously,⁴ hence only a brief description is presented here. All starting materials were used as received, including 1-methylimidazole and 1-methylpyrrolidine (both from Acros Organics), 3-chloropropyltrimethylsilane (Gelest), potassium bis(fluorosulfonyl)amide (Kanto Kagaku), lithium bis(trifluoromethylsulfonyl)amide (Kanto Kagaku), and lithium bis(pentafluoroethanesulfonyl)amide (Kishida Kagaku). First, chloride salts were obtained by the quaternization of either 1-methylimidazolium or 1-methylpyrrolidinium with 3-chloropropyltrimethylsilane, typically in acetonitrile solutions at 353 K for 48 h under an argon atmosphere. Appropriate purifications were performed for the product chloride salts, including washing with ethyl acetate, recrystallization, and decolorizing with activated charcoal. The Si-ILs were prepared from the corresponding chloride salts by ion exchange with the lithium or potassium salts K^+/FSI^- , $\text{Li}^+/\text{NTf}_2^-$, or $\text{Li}^+/\text{BETI}^-$. The ILs obtained were washed with distilled water several times until they passed the AgNO_3 test and were again decolorized with activated charcoal. Characterization of the samples was done using ^1H , ^{13}C , and ^{19}F NMR spectroscopies.

High-Energy X-ray Diffraction Experiments

The X-ray scattering experiments were carried out at sector 11-ID-B of the Advanced Photon Source, as described previously.^{47,52,53} Briefly, the ILs are filled in 3 mm glass NMR tubes under an argon atmosphere and then flame sealed. The X-ray beam with wavelength of 0.21140 Å is directed on the sample tube, and the 2-D X-ray scattering pattern is recorded using a Perkin-Elmer detector. Each sample is exposed under X-ray beam for a total time of 3 minutes. In each case the sample to detector distance is calibrated using a powder CeO₂ sample, and is approximately 22.7 cm. The 2D scattering pattern is integrated from center to edge using Fit2D software⁵⁴ to obtain scattering intensity over scattering vector q . The X-ray structure factor $S(q)$ is obtained using PDFgetX2 program from Qiu *et al.* during which many corrections are done including the Compton scattering and the subtraction of background of empty tubes.⁵⁵

Molecular Dynamics Simulations

The structure of ionic liquids are also studied using molecular dynamics (MD) simulations using the Gromacs 5.0.4 package⁵⁶⁻⁵⁸ with GPU acceleration. All settings and equilibration protocols are identical to the previous work.⁴⁷ Calculation of the liquid structure factors $S(q)$ was done using Equation 1, as described previously.^{39,41,47} Complete details of the simulation methods are provided in the Supplementary Material.

$$S(q) = \frac{\rho_0 \sum_i^n \sum_j^n f_i(q) f_j(q) \int_0^\infty 4\pi r^2 (g_{ij}(r) - 1) \frac{\sin qr}{qr} W(r) dr}{[\sum_i^n x_i f_i(q)]^2} \quad (1)$$

In this equation, ρ_0 is the box number density, $g_{ij}(r)$ is the radial distribution function between atom types i and j , x_i and x_j are the molar fractions of atoms i and j , and $f_i(q)$ and $f_j(q)$ are the atomic form factors for atom types i and j .^{59,60} The Lorch window function $W(r) = \sin(2\pi r/L)/(2\pi r/L)$ is used to account for the finite box sizes.^{44,61,62}

As described by Santos *et al.*, the total structure factor $S(q)$ can be partitioned into ionic contributions, as shown in Eq. 2,³⁹

$$S(q) = S_{c-c}(q) + S_{a-c}(q) + S_{c-a}(q) + S_{a-a}(q) \quad (2)$$

where a and c denote anionic and cationic contributions, respectively.

Kashyap *et al.* showed that $S(q)$ can be further deconstructed into sub-ionic partitions, including the interactions between anions, and cationic heads and tails, as shown in Eq. 3,⁴⁴

$$S(q) = S_{h-h}(q) + S_{t-t}(q) + S_{a-a}(q) + 2S_{h-a}(q) + 2S_{t-a}(q) + 2S_{h-t}(q) \quad (3)$$

where h and t indicate cationic head and tail contributions, respectively. The partitioning schemes for $S(q)$ are directly related to the original partitioning of binary mixtures of hard spheres described by Ashcroft and Langreth,⁶³ which are a formal inversion of the partitioning of the pair distribution described by Lebowitz.⁶⁴ For more strongly amphiphilic ILs, a polar/apolar partitioning of $S(q)$ can be quite useful.¹² However, since the Si-ILs do not have apolar tails, this polar/apolar partitioning is not used here.

The OPLS-AA^{65,66} based transferable force field by Canongia Lopes and Pádua (CL&P force field) are used for this simulation.⁶⁷⁻⁷⁰ The missing parameters are calibrated using the same method as described previously.⁴⁷ Details of the force fields used are given in the Supplementary Material.

Viscosity and Diffusivity Measurements

IL viscosities were measured in Kanazawa using a Brookfield LVDV-II cone-and-plate viscometer under atmospheric conditions. The temperature was controlled between 288.2 K and 368.2 K with ± 0.1 K accuracy. The standard deviation for a series of measurements of viscosity standards is ± 0.5 mPa-s.

The anionic and cationic diffusivities are measured using pulse-gradient spin echo (PGSE) NMR experiments^{71,72} using a bipolar pulse pair stimulated echo (D-BPP-STE) pulse sequence⁷³ as described previously.^{52,53} For diffusion measurements, the 3 mm NMR tubes, used later for the X-ray experiments, are directly placed inside a standard 5 mm NMR tube containing the D₂O for deuterium spin-locking. Spin echo intensities are obtained by measuring the spin-echo intensities for a set of 15-20 different magnetic field gradient strengths. Self-diffusion coefficients are obtained from these data using the analysis methods described previously.^{52,53} The field gradient is generated using a Doty Scientific model 16-38 diffusion probe on a 400 MHz Varian DirectDrive spectrometer. The gradient is calibrated to the diffusion coefficient of HDO in a standard D₂O sample to be 1.9×10^{-9} m²/s at 298 K.⁷⁴

Because the anions contain only ^{19}F atoms and no protons, and the cations contain multiple protons but no fluorines, the unique diffusivities for anions and cations are measured using ^{19}F and ^1H signals, respectively. The diffusivities for each peak in NMR spectra are analyzed, and the diffusion coefficient of the molecule is obtained by averaging them. Diffusivities measured for different atoms on the same molecule differ by less than 10%.

RESULTS AND DISCUSSION

Structure of silicon substituted ionic liquids

The simulated and experimental densities of the ILs studied are shown in Table I. The simulated density is systematically $\sim 7\%$ larger than experimental values. The IL densities estimated using CL&P force field is usually larger for most imidazolium and pyrrolidinium ionic liquids.⁷⁵ According to our previous experience, good match between experimental and simulated structure factors can still be achieved though there are small discrepancies in the ionic liquid densities.^{44,67}

TABLE I. Simulated and experimental densities (in g cm^{-3}), structure factors and experimental viscosities (in $\text{mPa}\cdot\text{s}$) for the four Si-ILs at 298 K.

IL	$\rho(\text{sim})$	$\rho(\text{exp})$ ^a	Viscosity ^b	Exp (sim) peak position in $S(q)$ (\AA^{-1})		
				adjacency	charge-charge correlation	FSDP
Si-C ₃ -mim ⁺ /FSI ⁻	1.335	1.248	92.3	1.30 (1.34)	–	0.37
Si-C ₃ -mim ⁺ /NTf ₂ ⁻	1.420	1.317	127.5	1.30 (1.34)	0.88 (0.90)	0.39
Si-C ₃ -mim ⁺ /BETI ⁻	1.494	1.394	287.0	1.27 (1.31)	0.84 (0.86)	0.41
Si-C ₃ -Pyr ⁺ /NTf ₂ ⁻	1.368	1.299	241.8	1.25 (1.27)	0.83 (0.83)	0.46

^a From Ref. 4; ^b Calculated from VFT fit parameters.

The structure factors obtained from high energy X-ray scattering experiments and from MD simulations are compared in Fig. 2. Structure factors obtained from the high-energy X-ray scattering data are plotted in red, while the MD results are plotted in blue. These results reveal significant shifts in the intensities and peak positions for the adjacency interactions, the charge-alternation correlations, and the FSDP for each of these four Si-ILs. Note that the scale of the $S(q)$ functions spans a range from 0 to 3. The q values for the adjacency

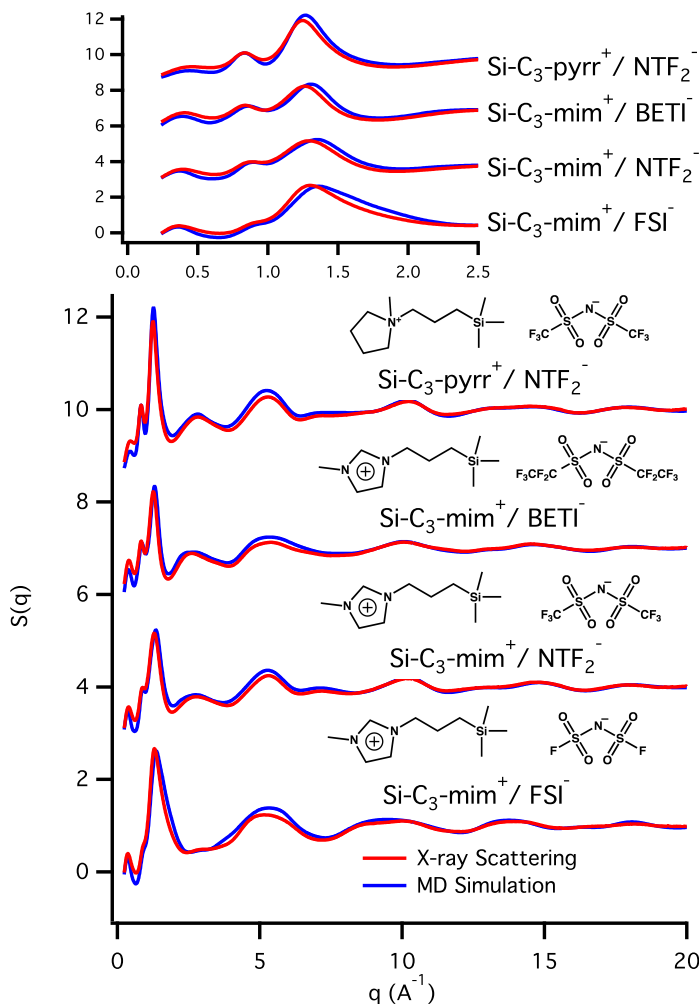


FIG. 2. The experimental and simulated structure factors of four ionic liquids. The top graph shows the details for the intermolecular regime of $S(q)$ between $0 < q < 2.5 \text{ \AA}^{-1}$. Arbitrary offsets of +3, +6 and +9 is applied to display the four $S(q)$ functions without overlap.

peaks are shown in Table I. The larger q values for each of the simulated peak positions are a direct consequence of the 7% over-estimation of the density. As discussed in our previous study of other Si-ILs having the NTf_2^- anion,⁴⁷ the incomplete agreement between calculated and measured peaks in the structure factors is likely arising from an imperfect form for the new Si parameters in the force field, since quantitative agreement for calculated vs. measured X-ray structure factors has been obtained for the existing CL&P parameters for NTf_2^- .⁶⁸

The ionic partitioning of $S(q)$ is accomplished by writing $S(q)$ according to Eq. 2. The

partial structure factor components of $S(q)$ are plotted in Fig. 3. Note that strong interference leads to partial $S(q)$ components that have significantly larger magnitudes than the observable total $S(q)$ function. Specifically, each of the four Si-ILs shows a maximum of about 3 in the total $S(q)$, while the partial $S(q)$ maxima can be as large as 8 for the case of Si-C₃-Pyrr⁺/NTf₂⁻. The adjacency peak is seen to arise from constructive interference from the anion-cation and cation-cation interactions, with smaller contributions from the anion-anion interactions. The charge-alternation signature is clear from the peak at $q=0.8 \text{ \AA}^{-1}$, where the anion-anion and cation-cation contributions make strong positive contributions that are ultimately offset and nearly canceled by the anti-peak resulting from the anion-cation contributions. It is worth noting that these anti-peaks cannot be directly observed in the total X-ray scattering, but their presence in the deconstructed partial structure factors is an unambiguous marker for underlying structure in the Si-ILs. The partial $S(q)$ functions for the Si-C₃-Pyrr⁺/NTf₂⁻ IL show the sharpest and most intense peaks, indicating a greater degree of ordering for this liquid relative to the corresponding imidazolium-cation Si-ILs.

Fig. 2 shows that the charge-charge correlation peak appears only as a shoulder at about 0.9 \AA^{-1} for Si-C₃-mim⁺/FSI⁻. The corresponding charge-charge correlation peaks in the X-ray structure functions for the other ILs are given in Table I. Since the charge-charge correlation is due to the second coordination shell interactions, we can obtain more information about this peak from the ionic partitioning of $S(q)$ from Fig. 3. The ionic interaction extrema in Fig. 3 are observed at q -values of approximately 0.90 \AA^{-1} for Si-C₃-mim⁺/FSI⁻, 0.84 \AA^{-1} for Si-C₃-mim⁺/NTf₂⁻, 0.81 \AA^{-1} for Si-C₃-mim⁺/BETI⁻ and 0.83 \AA^{-1} for Si-C₃-Pyrr⁺/NTf₂⁻. From the head-tail-anion partitioning in Fig. 4 we found that the charge-charge correlation peak is dominated by the interactions between anions and cation heads, and all interactions involving cation tails have a small effect on this peak, which indicates that the charge ordering is primarily determined by the polar parts of the molecules.⁴⁴

The cationic $-(\text{CH}_2)_3\text{Si}(\text{CH}_3)_3$ tail on both Si-C₃-mim⁺ and Si-C₃-Pyrr⁺ is sufficiently long to give rise to a clear FSDP, though the peak is broader and attenuated for the case of Si-C₃-Pyrr⁺/NTf₂⁻. From the ionic partitioning in Fig. 3 we observe that the FSDP is mainly arising from a positive-going anion-anion peak offset by a cation-anion anti-peak. These results are quite similar to the observations of the FSDP for ILs with hydrocarbon cationic tail reported previously.^{14,18–21,26,40,42–44,76}

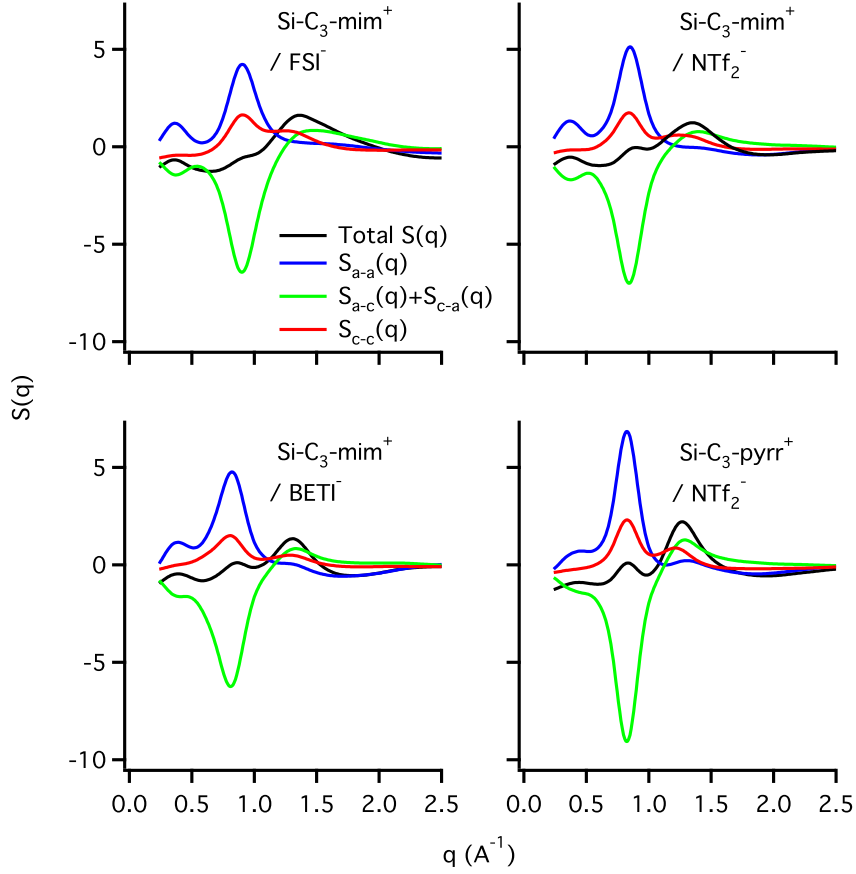


FIG. 3. The partial structure factors from ionic partitioning of $S(q)$ according to Eq. 2.

Further partitioning of $S(q)$ into sub-ionic categories is done using $S(q)$ in the form given by Eq. 3. The resulting total and partial $S(q)$ curves are shown in Fig. 4. The significantly larger electron density for the anions than the cations in this set of four Si-ILs is the reason that the scale for the sub-ionic components involving the anion are about a factor of three larger in magnitude than for purely cation-cation types of interactions. Specifically, the anion-anion (a-a), cationic head group-anion (h-a/a-h) and cationic tail group-anion (a-t/t-a) interactions are more intense than the cation-only interactions such as head-tail (h-t/t-h), tail-tail (t-t) and head-head (h-h). Note that the charge-alternation peak in $S(q)$ shows the strongest and sharpest contributions for the Si-C₃-Pyrr⁺/NTf₂⁻ IL, while the contributions to the FSDP intensity are strongest for the Si-C₃-mim⁺/NTf₂⁻ IL. In the ionic partitioning of $S(q)$ in Fig. 3 one sees that the FSDP consists primarily of anion-anion interactions, while the cation-cation interactions seem to have little effect on this peak. However, the sub-ionic partitioning of $S(q)$ shown in Fig. 4 shows that this is indeed a cancellation

between positive head-head and tail-tail interactions with a negative contribution of head-tail interaction. This illustrates the complex nature of the interactions in the intermediate range order in these ILs.

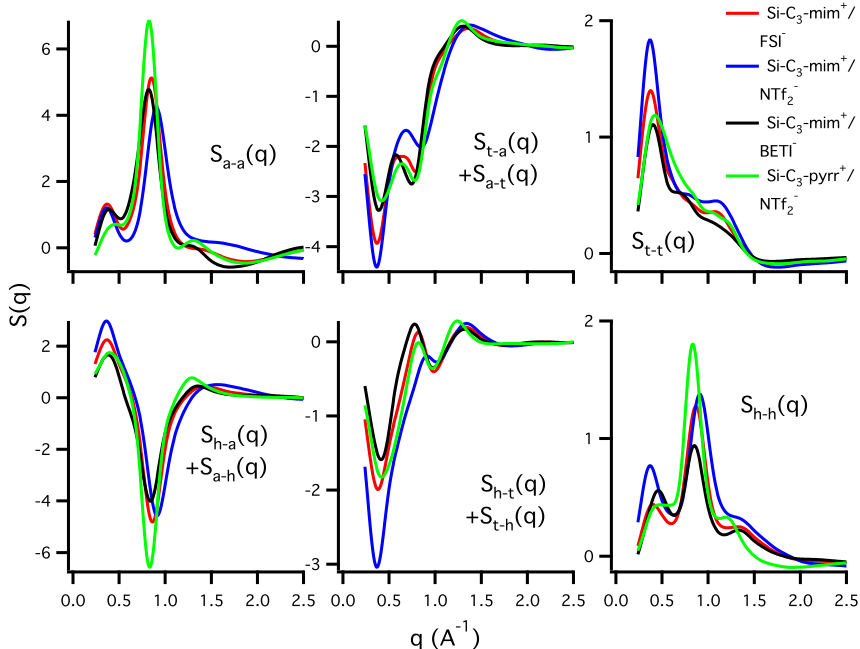


FIG. 4. Partial structure factors for partitioning of $S(q)$ into sub-ionic cation-head/cation-tail/anion interactions as per Eq. 3.

Spatial Distribution Functions of Anions and Cations

The spatial distribution of anions around cations for four ionic liquids are shown in Figs. 5 and 6. The spatial distributions are analyzed from simulation trajectory using TRAVIS software⁷⁷ and visualized using VMD.⁷⁸ In Fig. 5, the positions of cationic terminal $\text{Si}(\text{CH}_3)_3$ groups are fixed, with the anionic probability density shown in blue and the distribution of positions of the cationic ring shown in the red isodensity. The cationic ring probability density appears as it does as a result of the three-fold near symmetry around the $\text{Si}-\text{CH}_2$ bond.

In Fig. 6, spatial distribution is shown for a fixed position of the cationic head group, including the ring and polar atoms bonded to it. The anionic spatial isodensity is again shown in blue, with the orange indicating the averaged positions of the cationic tetra-

methylsilyl groups. These anionic distributions are similar to those we reported recently for Si-mim⁺/NTf₂⁻ and Si-pyrr⁺/NTf₂⁻, respectively.⁴⁷ This anion distribution obtained using classical potentials is remarkably similar to the results from quantum calculations.⁷⁹ For the four Si-ILs reported here, the anionic density is more centered around the cationic ring, because of the longer propylene linker. Despite the changes in anion size for the three ILs with Si-C₃-mim⁺ the FSI⁻, NTf₂⁻, and BETI⁻ anions, the shapes of these spatial distributions are nearly identical for these three Si-ILs. The distribution shape of anions in these ILs are similar to Si-mim⁺/NTf₂⁻ and Si-pyrr⁺/NTf₂⁻, while the anion distribution is more favor the ring, due to the longer alkyl chain.

Fig. 7 is the spatial distribution function of cations (red) and anions (blue) around anions. The spatial distributions for both Si-C₃-mim⁺/NTf₂⁻ and Si-C₃-Pyrr⁺/NTf₂⁻ are similar. Rather different spatial distributions are obtained for the Si-ILs for Si-C₃-mim⁺ paired with the FSI⁻ and BETI⁻ anions. From the spatial distribution for Si-C₃-mim⁺/BETI⁻ one observes that the coordination shell of cations forms a ring over the BETI⁻ anion center, and the cations are repelled by the anionic fluorocarbon groups.

Anion Effects on the Si-IL Structure

The adjacency peak shapes and positions in $S(q)$ do not show a consistent trend as the anion size is increased on going from FSI⁻ to NTf₂⁻ to BETI⁻. Despite the larger volume of the NTf₂⁻ relative to the FSI⁻ anion, the adjacency peak position for Si-C₃-mim⁺/NTf₂⁻ is at the same position as for Si-C₃-mim⁺/FSI⁻, while Si-C₃-mim⁺/BETI⁻ shifts to only a slightly lower value of q . The adjacency peaks for Si-C₃-mim⁺/NTf₂⁻ and Si-C₃-mim⁺/BETI⁻ have approximately same amplitudes, while the amplitude for the Si-C₃-mim⁺/FSI⁻ adjacency peak is significantly larger. Considering the effective ion pair volumes calculated from the experimental density, the ion pair volumes with Si-C₃-mim⁺ are 470 Å³ for FSI⁻, 559 Å³ for NTf₂⁻, and 642 Å³ for BETI⁻. This difference in ion pair volumes should lead to concomitant shifts in the adjacency peak, which are not observed. We believe that this different is probably due to the change of local packing of the IL structure. Contributions to the adjacency peak arise not only from the coordination of differently charged ions, but also from the contract of tail groups in the nano-segregated domains.^{44,80} The position of the FSDP reveals that the nano-domain for Si-C₃-mim⁺/FSI⁻ is larger than

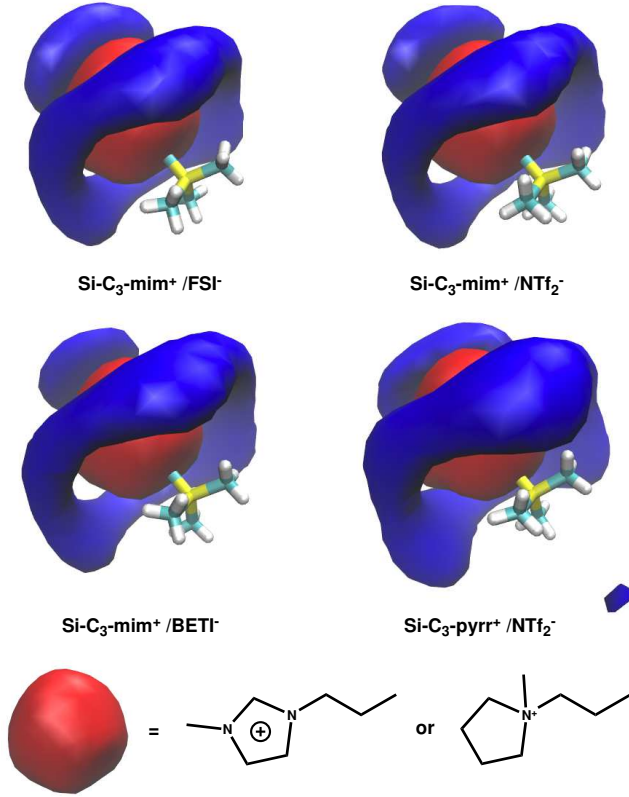


FIG. 5. The intermolecular spatial distribution of anions (blue) and cationic head groups (red) around cation tails for fixed positions of the $\text{Si}(\text{CH}_3)_3$ groups; the averaged ring positions for all 1,000 ion pairs in the simulation box are shown. The isodensity values for the anions are 2.35 nm^{-3} for FSI^- , 2.8 nm^{-3} for $\text{Si-C}_3\text{-mim}^+/\text{NTf}_2^-$, 2.0 nm^{-3} for BETI^- , and 2.1 nm^{-3} for $\text{Si-C}_3\text{-Pyrr}^+/\text{NTf}_2^-$.

for $\text{Si-C}_3\text{-mim}^+/\text{NTf}_2^-$, so in $\text{Si-C}_3\text{-mim}^+/\text{FSI}^-$ the contact of cation tails may be playing a more important role than in $\text{Si-C}_3\text{-mim}^+/\text{NTf}_2^-$, which in turn may lead to an adjacency peak shift. From Figs. 5 and 6 we also find evidence that the anion favors the cationic tail more than the ring for $\text{Si-C}_3\text{-mim}^+/\text{FSI}^-$.

The intensity of the charge-charge correlation peak in $\text{Si-C}_3\text{-mim}^+/\text{NTf}_2^-$ is smaller than for $\text{Si-C}_3\text{-mim}^+/\text{BETI}^-$, while $\text{Si-C}_3\text{-mim}^+/\text{FSI}^-$ only shows a shoulder in this q regime. A larger charge-charge correlation peak intensity here does not necessarily indicate a stronger anion-anion interaction, because the X-ray scattering cross section increases for the anions with more heavy atoms. The position of the charge-charge correlation peak as well as the position of charge correlation from ionic partitioning of $S(q)$ shows a shift to lower q values

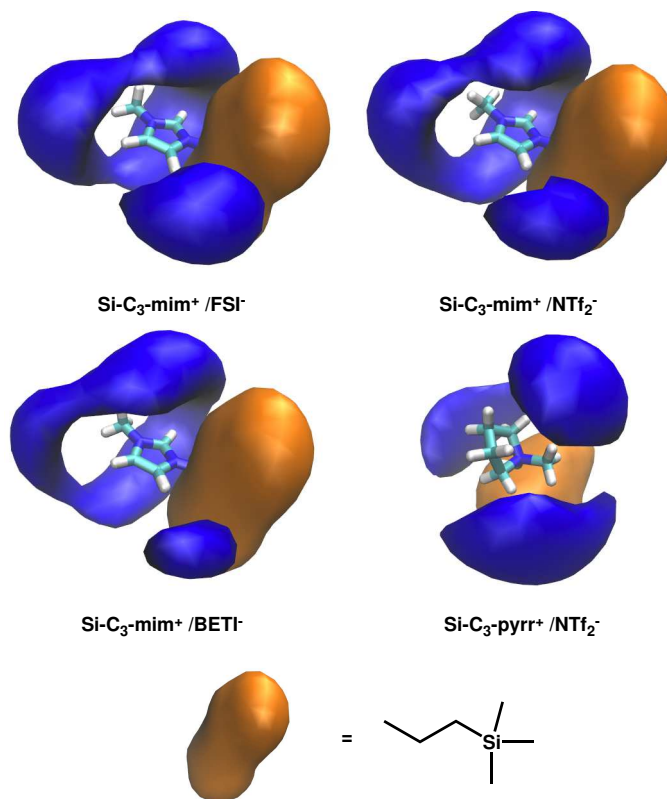


FIG. 6. The spatial distribution of anions around cations, where the ring position is fixed and the cationic tail positions are averaged for the 1,000 ion pairs in the simulation box. The isovalues for the anion number densities are 2.6 nm^{-3} for $\text{Si-C}_3\text{-mim}^+ / \text{FSI}^-$, 3.2 nm^{-3} for $\text{Si-C}_3\text{-mim}^+ / \text{NTf}_2^-$, 2.2 nm^{-3} for $\text{Si-C}_3\text{-mim}^+ / \text{BETI}^-$, and 2.5 nm^{-3} for $\text{Si-C}_3\text{-pyrr}^+ / \text{NTf}_2^-$.

for the large anions, as expected. However, the ionic partitioning of the structure factors shows that for all cation-cation, anion-anion, cation-anion interactions, the trend of peak amplitudes for $S(q)$ scales as $\text{Si-C}_3\text{-mim}^+ / \text{NTf}_2^- < \text{Si-C}_3\text{-mim}^+ / \text{FSI}^- < \text{Si-C}_3\text{-mim}^+ / \text{BETI}^-$.

When the size of the anion increases from FSI^- to NTf_2^- to BETI^- , the intensity of the FSDP in $S(q)$ increases while the peak shifts to larger q . Instead of taking part in forming a non-polar domain in IL structure, the fluorine- or perfluorocarbon ends of the anion prevent the non-polar domains in the ILs from growing. The FSDP intensity follows the trend $\text{FSI}^- < \text{NTf}_2^- < \text{BETI}^-$ because of the larger X-ray scattering cross section for the anion.

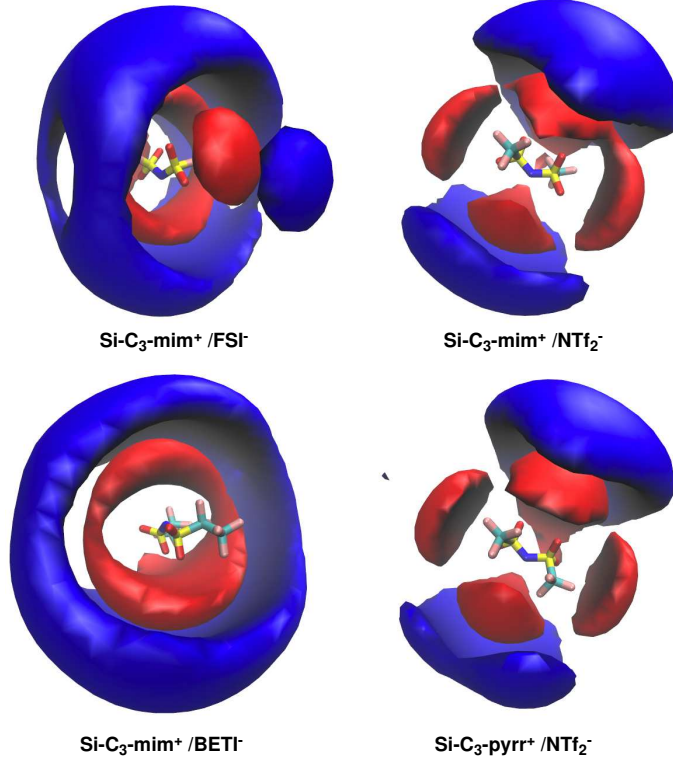


FIG. 7. Spatial distributions around the Si-IL anions, for fixed angles of the anionic S–N–S bond angles. The cationic (anionic) isodensity values are 2.05 (2.00) nm^{-3} for Si-C₃-mim⁺/FSI⁻; 2.50 (2.40) nm^{-3} for Si-C₃-mim⁺/NTf₂⁻; 1.80 (1.65) nm^{-3} for Si-C₃-mim⁺/BETI⁻; 2.00 (2.00) nm^{-3} for Si-C₃-Pyrr⁺/NTf₂⁻.

Cationic Tail Length and Polarity Effects on IL Structure

How the polarity and chain length will affect the silicon-substituted ILs can be studied by comparing the structures of Si-C₃-mim⁺/NTf₂⁻ and Si-C₃-Pyrr⁺/NTf₂⁻ with those of Si-mim⁺/NTf₂⁻, SiOSi-mim⁺/NTf₂⁻ and Si-pyrr⁺/NTf₂⁻ in Ref. 47. Changing the cationic functionality from the trimethylsilylmethyl group to the trimethylsilylpropyl group leads to the introduction of a FSDP in $S(q)$ because the latter $-(\text{CH}_2)_3\text{Si}(\text{CH}_3)_3$ tail is long enough. The FSDP in Si-C₃-mim⁺/NTf₂⁻ is more intense and occurs at lower q value of 0.39 \AA^{-1} , compared to $q = 0.41 \text{\AA}^{-1}$ for SiOSi-mim⁺/NTf₂⁻, which has the same chain length. This indicates a larger and stronger nano-aggregation of side chains than in Si-C₃-mim⁺/NTf₂⁻.

The adjacency peak in $S(q)$ is found at $q = 1.28 \text{\AA}^{-1}$ for Si-mim⁺/NTf₂⁻ and 1.27 \AA^{-1} for Si-pyrr⁺/NTf₂⁻. We found that increasing cation chain length will lead the adjacency peak moving to higher q value, which indicates a smaller Bragg domain for an ion pair. This is in

contrast to the larger molecular volume of the longer chain cation. This may be explained by the differences in the packing in the ionic liquids. As we have discussed for the spatial distribution in Figs. 5 and 6, one clearly sees that anions show increased correlation with the cationic rings, which may lead to decreased distances between anions and cationic head groups.

The charge-charge correlation peak in $S(q)$ is observed at $q= 0.87$ (0.90) \AA^{-1} for Si-mim⁺/NTf₂⁻ and 0.83 (0.85) \AA^{-1} for Si-pyrr⁺/NTf₂⁻ while the second coordination interactions analyzed from the partial $S(q)$ are found at $q= 0.83$ for Si-mim⁺/NTf₂⁻ and 0.82 for Si-pyrr⁺/NTf₂⁻. Though the position of charge-charge correlation peak changes noticeably on changing from the trimethylsilylmethyl group to the trimethylsilylpropyl group, the average distance charge-charge interactions from $S(q)$ partitioning do not have a significant change. Since charge-charge correlation peak partially overlaps with the adjacency peak, this peak shift may mainly be related to different adjacency peak broadening.

Structural Differences for Imidazolium vs. Pyrrolidinium Cations

The FSDP in $S(q)$ for the Si-C₃-mim⁺/NTf₂⁻ Si-IL is much more intense than for Si-C₃-Pyrr⁺/NTf₂⁻ and is observed at a lower q value. This is consistent with the behavior manifested by ILs having hydrocarbon side chains, because C[n]-imidazolium cations have a longer effective length than the homologous C[n]-pyrrolidiniums.^{43,44,81}

For the Si-ILs having $-\text{CH}_2\text{Si}(\text{CH}_3)_3$ groups, the position of the adjacency peak in $S(q)$ is the same for both Si-mim⁺/NTf₂⁻ and Si-pyrr⁺/NTf₂⁻.⁴⁷ However, for the $-(\text{CH}_2)_3\text{Si}(\text{CH}_3)_3$ cationic group, the imidazolium-cation Si-C₃-mim⁺/NTf₂⁻ adjacency peak is observed at a lower value of q relative to the pyrrolidinium-cation Si-C₃-Pyrr⁺/NTf₂⁻. The peak positions for each of these interactions for Si-C₃-Pyrr⁺/NTf₂⁻ IL are shifted to lower values of q relative to the three ILs with the Si-C₃-mim⁺-cation ILs, indicating that the former pyrrolidinium-cation IL has larger spatial dimensions for each of the three inter-molecular domains.

From the ionic partitioning of $S(q)$ presented in Fig. 3 we found that the pyrrolidinium Si-ILs have much sharper ionic partial structure factors do the imidazolium ILs. One sees in Fig. 4 that the same holds true for the sub-ionic partitioning of $S(q)$.

Diffusivities of Si-ILs

Self-diffusion coefficients for anions and cations in ILs have long been measured using the PG-SE NMR method.⁸²⁻⁸⁵ These measurements complement the measurements of other transport properties including conductivity and viscosity, as these measure the total flux of ions. By comparing self-diffusion coefficients obtained from PG-SE NMR measurements with conductivity data, the ionicity, or degree of independent motion of the ions in the IL can be determined.⁸⁶ The diffusivities of anions, cations and solutes in ILs do not precisely scale with hydrodynamic models, but rather with a fractional Stokes-Einstein equation.⁸⁷ We have observed this behavior previously for the Si-IL Si-mim⁺ and the hydrocarbon analog C-mim⁺, both with the BF₄⁻ and NTf₂⁻ anions.³ It is worth noting that neutral solutes in ILs experience a significantly lower friction than do the ions, leading to transport much faster than expected based on hydrodynamic predictions.^{52,53,88}

The anionic and cationic diffusivities for a set of 7 Si-ILs and one hydrocarbon-tailed homolog were measured using the PG-SE NMR technique. The diffusivities measured at 298, 303 and 308 K are plotted in Fig. 8. A larger spatial extent for either the anion or the cation leads to decreased diffusivities for both anions and cations. More polar and flexible side chains can increase the diffusivities of both anions and cations. The anion in SiOSi-mim⁺/NTf₂⁻ diffuses approximately as fast as in Si-mim⁺/NTf₂⁻. For the case of a common anion for a pair of Si-ILs, the imidazolium cation IL generally displays a diffusivity (and inverse viscosity) that is about a factor of two larger than the homologous IL with a pyrrolidinium cation. A similar trend is observed for ILs with hydrocarbon side chains.⁸⁸

The viscosities for the Si-C₃-mim⁺ and Si-C₃-Pyrr⁺ Si-ILs are plotted in Fig. 9, shown with fits to the Vogel-Fulcher-Tammann (VFT) equation. The VFT fit parameters are provided in the Supplementary Material. These viscosity data are used in calculating diffusivity estimates from the Sutherland-Stokes-Einstein equation, $D = k_B T / (6\pi\eta R)$. Here T is the absolute temperature, η the shear viscosity, and R the effective radius of the diffusing species. R is estimated from the molecular volume obtained from a geometry-optimized gas-phase structure at the HF/6-31G(d) level of electronic structure. In Fig. 10, we plot the diffusivities measured using PG-SE NMR against the calculated hydrodynamic diffusivity estimates. The graph on the left in Fig. 10 plots the measured vs. calculated self-diffusion coefficients for the anions, while the graph on the right plots the same values for the cations.

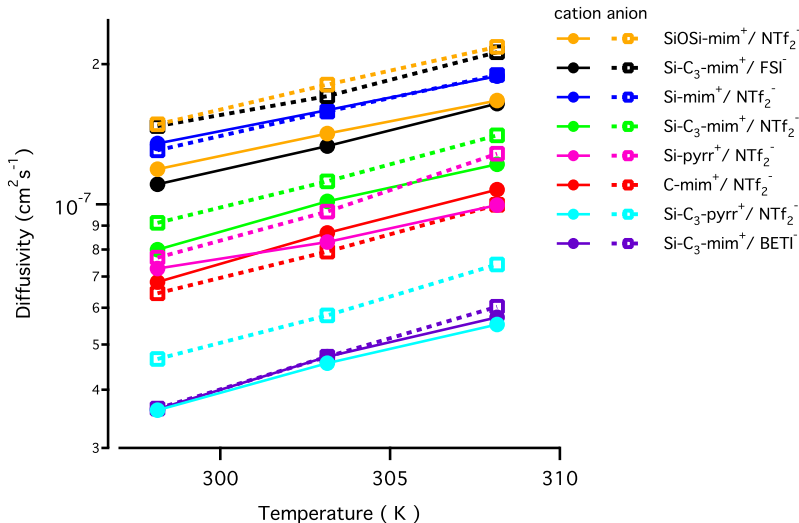


FIG. 8. The diffusivities of ionic liquid cations and anions measured by PG-SE NMR technique. Solid symbols indicate cationic diffusivities and open symbols are for anionic diffusivities. Lines serve only to connect the data points.

In addition to the 24 data points for the 7 Si-ILs and for C-mim⁺/NTf₂⁻, we also include diffusivities for several ILs with bis-(fluorinated sulfonyl)amide anions that have typical hydrocarbon-functionalized cations, such as Im_{4,1}⁺, Pyr_{4,1}⁺, and related species.^{83–85,89,90} In these graphs, blue data points represent the silicon containing ionic liquids (Si-ILs) and red points are for the ILs with hydrocarbon-tailed cations that do not contain any silicon atoms. The object in Fig. 10 is to quantitatively compare the relative behaviors of anion and cation self-diffusion after normalizing for ion size and bulk viscosity. The anionic self-diffusion coefficients plotted in the graph on the left side of Fig. 10 behave as expected. The graphs of the cationic self-diffusion coefficients shown on the right side of Fig. 10 show that the trend line for the prototypical dialkyl- imidazolium and pyrrolidinium cations also display a consistent scaling once normalized for viscosity and size, but that the slope of the same trend line for the Si-ILs is only 2/3 the value of the hydrocarbon-tailed IL cations. The straight lines in Fig. 10 are linear fits of the points, and the slopes can be found in the Supplementary Material. This result points out that though the anionic and cationic self-diffusivities must be somewhat correlated in any IL, the Si-IL cations are experiencing a reduced friction compared to the homologous classes of hydrocarbon-cation ILs- they are in fact more slippery. Most intriguing is that this slipperiness seems to be a property belonging only to the cation in the Si-ILs, not to the anion in the same liquid. This opens up the

question of whether the class of Si-ILs may in fact be superior for various tribological and heat-transfer applications. It will be of great interest to explore the mechanisms of relative diffusivities of Si-IL anions and cations using molecular dynamics simulations,⁹¹ in order to correlate structure with transport properties.¹³

The CL&P force field used here can lead to quantitative agreement between experiments and simulations for structural properties. However, CL&P often leads to up to an order of magnitude error for the calculation of self-diffusion coefficients in ILs.⁷⁵ Fully polarizable or *ab initio* methods^{29,92–96} are often required to accurately reproduce observable properties such as diffusivities or viscosity. Scaled-charge methods can be used to approximate the polarization effects on the ions,^{97–100} since charge transfer plays an important role in determining ion diffusivities.^{100,101}

Köddermann *et al.* tuned the Lennard-Jones parameters in the force field to more accurately reproduce dynamical properties.⁷⁵ We simulated the diffusivities of Si-mim⁺/NTf₂⁻ and C-mim⁺/NTf₂⁻ using this force field, using the final equilibrated boxes for Si-mim⁺/NTf₂⁻ and C-mim⁺/NTf₂⁻ from previous work for the initial geometries.⁴⁷ Only the van der Waals parameters in the force field are replaced by the parameters from Koeddermann *et al.* while all other CL&P parameters are unchanged. The simulations are done using the double precision GROMACS-4.5.5 package.^{57,58} The boxes are further equilibrated for 5 ns using Nosé-Hoover thermostat^{102,103} and Parrinello-Rahman barostat¹⁰⁴. The final production run is at constant energy and volume (NVE) for 8 ns. The simulated diffusivities are 1.42 (1.351) $\times 10^{-7}$ cm²/s for Si-mim⁺ and 1.28 (1.306) 10^{-7} cm²/s for NTf₂⁻ in Si-mim⁺/NTf₂⁻; 1.78 (0.681) 10^{-7} cm²/s for C-mim⁺ and 1.46 (0.644) 10^{-7} cm²/s for NTf₂⁻ in C-mim⁺/NTf₂⁻. The diffusivities from PG-SE NMR experiments from this work are given in parentheses. The simulated diffusivities for Si-mim⁺/NTf₂⁻ are similar to experiments, but this trend is not followed by C-mim⁺/NTf₂⁻. Further tuning of the force field will be needed in the future to obtain the correct trends in diffusivities.

CONCLUSIONS

Using high-energy X-ray diffraction and molecular dynamics simulations, we measured and calculated the bulk liquid structures for four silicon containing ionic liquids, Si-C₃-mim⁺/FSI⁻, Si-C₃-mim⁺/NTf₂⁻, Si-C₃-mim⁺/BETI⁻ and Si-C₃-Pyrr⁺/NTf₂⁻ and com-

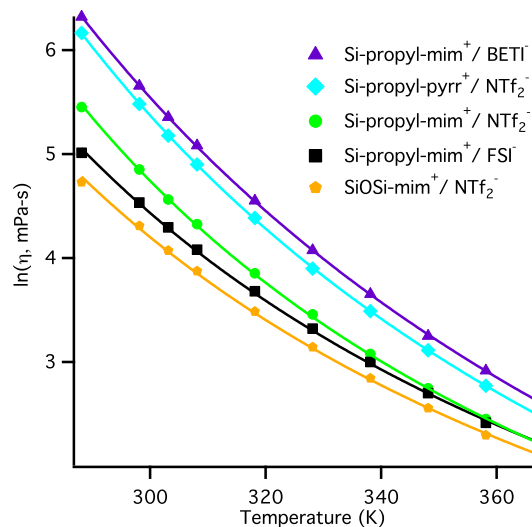


FIG. 9. Shear viscosities for five of ionic liquids plotted vs. temperature. Lines are fits to the VFT equation; the fit parameters are given in the Supplementary Information.

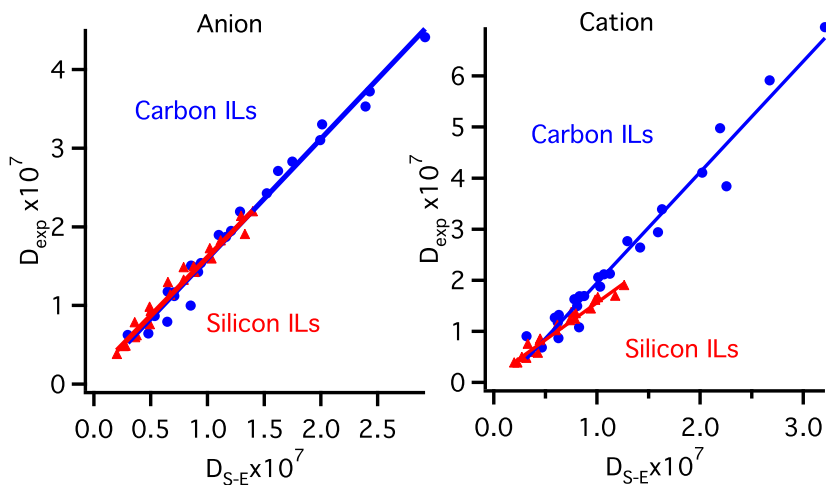


FIG. 10. Plots of diffusivities of anions (left) and cations (right) predict by the (Sutherland)-Stokes-Einstein Equation vs. diffusivities measured by PG-SE NMR. Red points are ionic liquids containing silicon from this work, blue points are ILs with hydrocarbon-substituted cations from this work and the literature.^{83–85,89,90} Linear fits to the data are shown.

pared them with other silicon or hydrocarbon side chain ILs including Si-mim⁺/NTf₂⁻, C-mim⁺/NTf₂⁻, SiOSi-mim⁺/NTf₂⁻ and Si-pyrr⁺/NTf₂⁻. We also measured the diffusivities and viscosities of these ionic liquids. We achieved good agreements between the structure factors $S(q)$ between experiments and simulations. We analyzed the effect of the anion

type, the tail group length/polarity and the head group type will affect ionic liquid on silicon-substituted ionic liquids structures.

The $-(\text{CH}_2)_3\text{Si}(\text{CH}_3)_3$ functional group on the cation is large enough to cause the emergence of a FSDP in the liquid structure factor for the IL. The resulting domain will be larger than that formed by the polar aggregation of a same length side chain in $\text{SiOSi-mim}^+/\text{NTf}_2^-$. Increasing the chain from the $-\text{CH}_2\text{Si}(\text{CH}_3)_3$ to the $-(\text{CH}_2)_3\text{Si}(\text{CH}_3)_3$ group will lead to a shift of the adjacency peak in $S(q)$ to larger values of q , indicating a smaller average intermolecular distance between the ions. This might be explained by the changes in liquid organization in the $-(\text{CH}_2)_3\text{Si}(\text{CH}_3)_3$ -tail domains, and the adjacency interactions between anions and cation heads. Increasing the cation chain length will generally decrease the diffusivities of ions, while a polar and flexible side chain generally enhances the diffusivity relative to an apolar side chain.

An anion with a larger fluorinated group changes the relative fraction of contributions to $S(q)$ from polar head groups vs. hydrophobic perfluorocarbon groups, which will in turn cause a shift of the adjacency peak to lower q values. The longer fluorinated segment in the anion will lead to a smaller intermediate-range-domain in the IL structure, as indicated by the FSDP shifting to higher q range.

We studied the relation between measured diffusivities measured by PG-SE NMR and predicted by the Sutherland-Stokes-Einstein Equation. We found that for sulfonylimide based anion ionic liquids with either silicon containing side chains or hydrocarbon side chains, there is a linear relation between the experimental and theoretical diffusion coefficients. For the anions, the IL with either silicon contained side chain or hydrocarbon side chain share a same scale factor, but for the cation diffusivity, the scaling factor of two type ILs are different.

SUPPLEMENTARY MATERIAL

See supplementary material for more detailed supplementary information on parametrization of the MD force fields for $\text{Si-C}_3\text{-mim}^+$ and $\text{Si-C}_3\text{-Pyrr}^+$; estimation of the anionic and cationic radii; and details on the tabulation of the literature diffusivities and viscosities used in Figs. 8 and 10.

ACKNOWLEDGMENTS

This work is supported by the NSF through grant CHE-1362272 to Rutgers University. Work in Kanazawa was supported in part by the Advanced Low Carbon Technology Research and Development Program (ALCA) (Grant number 2100040), the Cross-ministerial Strategic Innovation Promotion Program (SIP), and the Center of Innovation Program Construction of next-generation infrastructure using innovative materials: Realization of safe and secure society that can coexist with the Earth for centuries from Japan Science and Technology Agency. High-energy X-ray experiments used resources of the Advanced Photon Source, a U.S. Department of Energy (DOE) Office of Science User Facility operated for the DOE Office of Science by Argonne National Laboratory under Contract No. DE-AC02-06CH11357. We thank APS beamline scientists, Dr. Olaf J. Borkiewicz, Kevin A. Beyer and Dr. Karena W. Chapman for their assistance in X-ray data collection. The authors thank Mr. Yuki Matsushita, Kanazawa University, for previous preparation of the Si-IL samples. We thank Professor Claudio J. Margulis and Dr. Juan Carlos Araque from the University of Iowa for helpful suggestions and access to computational resources. We thank Dr. Nagarajan Murali at Rutgers University for the assistance with the PG-SE NMR experiments.

REFERENCES

- ¹H. Shirota and E. W. Castner, Jr., “Why Are Viscosities Lower for Ionic Liquids with $\text{CH}_2\text{Si}(\text{CH}_3)_3$ vs. $\text{CH}_2\text{C}(\text{CH}_3)_3$ Substitutions on the Imidazolium Cations?” *J. Phys. Chem. B* **109**, 21576–21585 (2005).
- ²H. Shirota, J. F. Wishart, and E. W. Castner, Jr., “Intermolecular Interactions and Dynamics of Room Temperature Ionic Liquids That Have Silyl- and Siloxy-Substituted Imidazolium Cations,” *J. Phys. Chem. B* **111**, 4819–4829 (2007).
- ³S. H. Chung, R. Lopato, S. G. Greenbaum, H. Shirota, E. W. Castner, Jr., and J. F. Wishart, “A nuclear magnetic resonance study of room temperature ionic liquids with $\text{CH}_2\text{Si}(\text{CH}_3)_3$ vs. $\text{CH}_2\text{C}(\text{CH}_3)_3$ substitutions on the imidazolium cations,” *J. Phys. Chem. B* **111**, 4885–4893 (2007).
- ⁴T. Endo, S. Nemugaki, Y. Matsushita, Y. Sakai, H. Ozaki, Y. Hiejima, Y. Kimura, and K. Takahashi, “Fast solute diffusivity in ionic liquids with silyl or siloxane groups studied

- by the transient grating method,” *Chem. Phys.* **472**, 128–134 (2016).
- ⁵H. Niedermeyer, M. A. A. Rani, P. D. Lickiss, J. P. Hallett, T. Welton, A. J. P. White, and P. A. Hunt, “Understanding siloxane functionalised ionic liquids,” *Phys. Chem. Chem. Phys.* **12**, 2018–2029 (2010).
- ⁶S. Bulut, M. A. A. Rani, T. Welton, P. D. Lickiss, and I. Krossing, “Preparation of $[\text{Al}(\text{hfp})_4]^-$ Based Ionic Liquids with Siloxane-Functionalized Cations and Their Physical Properties in Comparison with Their $[\text{Tf}_2\text{N}]^-$ Analogues,” *ChemPhysChem* **13**, 1802–1805 (2012).
- ⁷J. E. Bara, T. K. Carlisle, C. J. Gabriel, D. Camper, A. Finotello, D. L. Gin, and R. D. Noble, “Guide to CO_2 Separations in Imidazolium-Based Room-Temperature Ionic Liquids,” *Ind. Eng. Chem. Res.* **48**, 2739–2751 (2009).
- ⁸A. S. Vuk, V. Jovanovski, A. Pollet-Villard, I. Jerman, and B. Orel, “Imidazolium-based ionic liquid derivatives for application in electrochromic devices,” *Sol. Energy Mater. Sol. Cells* **92**, 126–135 (2008).
- ⁹V. Jovanovski, E. Stathatos, B. Orel, and P. Lianos, “Dye-sensitized solar cells with electrolyte based on a trimethoxysilane-derivatized ionic liquid,” *Thin Solid Films* **511-512**, 634637 (2006).
- ¹⁰J. Tan and S. Feng, “Effect of Counterions on Micellization of Pyrrolidinium Based Silicone Ionic Liquids in Aqueous Solutions,” *J. Chem. Eng. Data* **59**, 1830–1834 (2014).
- ¹¹R. Hayes, G. G. Warr, and R. Atkin, “Structure and Nanostructure in Ionic Liquids,” *Chem. Rev.* **115**, 6357–6426 (2015).
- ¹²H. K. Kashyap, J. J. Hettige, H. V. R. Annapureddy, and C. J. Margulis, “SAXS anti-peaks reveal the length-scales of dual positive-negative and polar-apolar ordering in room-temperature ionic liquids,” *Chem. Commun.* **48**, 5103–5105 (2012).
- ¹³J. C. Araque, S. K. Yadav, M. Shadeck, M. Maroncelli, and C. J. Margulis, “How Is Diffusion of Neutral and Charged Tracers Related to the Structure and Dynamics of a Room-Temperature Ionic Liquid? Large Deviations from Stokes-Einstein Behavior Explained,” *J. Phys. Chem. B* **119**, 7015–7029 (2015).
- ¹⁴S. M. Urahata and M. C. C. Ribeiro, “Structure of ionic liquids of 1-alkyl-3-methylimidazolium cations: A systematic computer simulation study,” *J. Chem. Phys.* **120**, 1855–1863 (2004).

- ¹⁵M. G. Del Popolo and G. A. Voth, “On the structure and dynamics of ionic liquids,” *J. Phys. Chem. B* **108**, 1744–1752 (2004).
- ¹⁶A. Triolo, O. Russina, R. Caminiti, H. Shirota, H. Y. Lee, C. S. Santos, N. S. Murthy, and E. W. Castner, Jr, “Comparing intermediate range order for alkyl- vs. ether-substituted cations in ionic liquids,” *Chem. Commun.* **48**, 4959–4961 (2012).
- ¹⁷O. Russina and A. Triolo, “New experimental evidence supporting the mesoscopic segregation model in room temperature ionic liquids,” *Faraday Discuss.* **154**, 97–109 (2012).
- ¹⁸O. Russina, A. Triolo, L. Gontrani, R. Caminiti, D. Xiao, J. Hines, Larry G., R. A. Bartsch, E. L. Quitevis, N. Pleckhova, and K. R. Seddon, “Morphology and intermolecular dynamics of 1-alkyl-3-methylimidazolium bis(trifluoromethane)sulfonylamide ionic liquids: structural and dynamic evidence of nanoscale segregation,” *J. Phys.: Condens. Matter* **21**, 424121 (2009).
- ¹⁹C. E. S. Bernardes, K. Shimizu, A. I. M. C. L. Ferreira, L. M. N. B. F. Santos, and J. N. C. Lopes, “Structure and Aggregation in the 1,3-Dialkyl-imidazolium Bis(trifluoromethylsulfonyl)imide Ionic Liquid Family: 2. From Single to Double Long Alkyl Side Chains,” *J. Phys. Chem. B* **118**, 6885–6895 (2014).
- ²⁰C. Hardacre, J. D. Holbrey, C. L. Mullan, T. G. A. Youngs, and D. T. Bowron, “Small angle neutron scattering from 1-alkyl-3-methylimidazolium hexafluorophosphate ionic liquids (C(n)mim PF₆, n=4, 6, and 8),” *J. Chem. Phys.* **133**, 074510 (2010).
- ²¹K. Fujii, R. Kanzaki, T. Takamuku, Y. Kameda, S. Kohara, M. Kanakubo, M. Shibayama, S. ichi Ishiguro, and Y. Umebayashi, “Experimental evidences for molecular origin of low-Q peak in neutron/x-ray scattering of 1-alkyl-3-methylimidazolium bis(trifluoromethanesulfonyl)amide ionic liquids,” *J. Chem. Phys.* **135**, 244502 (2011).
- ²²Y. Umebayashi, W.-L. Chung, T. Mitsugi, S. Fukuda, M. Takeuchi, K. Fujii, T. Takamuku, R. Kanzaki, and S.-i. Ishiguro, “Liquid Structure and the Ion-Ion Interactions of Ethylammonium Nitrate Ionic Liquid Studied by Large Angle X-Ray Scattering and Molecular Dynamics Simulations,” *J. Comput. Chem. Jpn* **7**, 125–134 (2008).
- ²³K. Fujii, S. Seki, S. Fukuda, T. Takamuku, S. Kohara, Y. Kameda, Y. Umebayashi, and S.-i. Ishiguro, “Liquid structure and conformation of a low-viscosity ionic liquid, N-methyl-N-propyl-pyrrolidinium bis(fluorosulfonyl) imide studied by high-energy X-ray scattering,” *J. Mol. Liq.* **143**, 64–69 (2008).

- ²⁴S. Fukuda, M. Takeuchi, K. Fujii, R. Kanzaki, T. Takamuku, K. Chiba, H. Yamamoto, Y. Umebayashi, and S.-i. Ishiguro, "Liquid structure of N-butyl-N-methylpyrrolidinium bis(trifluoromethanesulfonyl) amide ionic liquid studied by large angle X-ray scattering and molecular dynamics simulations," *J. Mol. Liq.* **143**, 2–7 (2008).
- ²⁵R. Kanzaki, T. Mitsugi, S. Fukuda, K. Fujii, M. Takeuchi, Y. Soejima, T. Takamuku, T. Yamaguchi, Y. Umebayashi, and S. Ishiguro, "Ion-ion interaction in room temperature ionic liquid 1-ethyl-3-methylimidazolium tetrafluoroborate studied by large angle X-ray scattering experiment and molecular dynamics simulations," *J. Mol. Liq.* **147**, 77–82 (2009).
- ²⁶K. Fujii, Y. Soejima, Y. Kyoshoin, S. Fukuda, R. Kanzaki, Y. Umebayashi, T. Yamaguchi, S.-i. Ishiguro, and T. Takamuku, "Liquid Structure of Room-Temperature Ionic Liquid, 1-Ethyl-3-methylimidazolium Bis-(trifluoromethanesulfonyl) Imide," *J. Phys. Chem. B* **112**, 4329–4336 (2008).
- ²⁷M. Kofu, M. Nagao, T. Ueki, Y. Kitazawa, Y. Nakamura, S. Sawamura, M. Watanabe, and O. Yamamuro, "Heterogeneous Slow Dynamics of Imidazolium-Based Ionic Liquids Studied by Neutron Spin Echo," *J. Phys. Chem. B* **117**, 2773–2781 (2013).
- ²⁸K. B. Dhungana, L. F. O. Faria, B. Wu, M. Liang, M. C. C. Ribeiro, C. J. Margulis, and E. W. Castner, Jr, "Structure of cyano-anion ionic liquids: X-ray scattering and simulations," *J. Chem. Phys.* **145**, 024503 (2016).
- ²⁹M. G. D. Pópolo, R. M. Lynden-Bell, and J. Kohanoff, "Ab Initio Molecular Dynamics Simulation of a Room Temperature Ionic Liquid," *J. Phys. Chem. B* **109**, 5895–5902 (2005).
- ³⁰J. J. Hettige, J. C. Araque, H. K. Kashyap, and C. J. Margulis, "Communication: Nanoscale structure of tetradecyltrihexylphosphonium based ionic liquids," *J. Chem. Phys.* **144**, 121102 (2016).
- ³¹K. Shimizu, M. F. C. Gomes, A. A. H. Pádua, L. P. Rebelo, and J. N. C. Lopes, "Three commentaries on the nano-segregated structure of ionic liquids," *J. Mol. Struct.: TheoChem* **946**, 7076 (2010).
- ³²K. Shimizu and J. N. C. Lopes, "Probing the structural features of the 1-alkyl-3-methylimidazolium hexafluorophosphate ionic liquid series using Molecular Dynamics simulations," *J. Mol. Liq.* **210**, 257–263 (2015).

- ³³K. Shimizu and J. N. C. Lopes, “Comparing the structure of different ionic liquid series: Bistriflamide v. hexafluorophosphate; pure v. equimolar mixtures,” *Fluid Phase Equilib.* **418**, 181–191 (2016).
- ³⁴O. Borodin, D. L. Price, B. Aoun, M. A. Gonzalez, J. B. Hooper, M. Kofu, S. Kohara, O. Yamamuro, and M.-L. Saboungi, “Effect of water on the structure of a prototype ionic liquid,” *Phys. Chem. Chem. Phys.* **18**, 23474–23481 (2016).
- ³⁵O. Russina, S. De Santis, and L. Gontrani, “Micro- and mesoscopic structural features of a bio-based choline-amino acid ionic liquid,” *RSC Adv.* **6**, 34737–34743 (2016).
- ³⁶S. Sharma, A. Gupta, and H. K. Kashyap, “How the Structure of Pyrrolidinium Ionic Liquids Is Susceptible to High Pressure,” *J. Phys. Chem. B* **120**, 3206–3214 (2016).
- ³⁷A. Mariani, O. Russina, R. Caminiti, and A. Triolo, “Structural organization in a methanol:ethylammonium nitrate (1:4) mixture: A joint X-ray/Neutron diffraction and computational study,” *J. Mol. Liq.* **212**, 947–956 (2015).
- ³⁸A. Mariani, M. Campetella, C. Fasolato, M. Daniele, F. Capitani, L. Bencivenni, P. Postorino, S. Lupi, R. Caminiti, and L. Gontrani, “A joint experimental and computational study on ethylammonium nitrate-ethylene glycol 1:1 mixture. Structural, kinetic, dynamic and spectroscopic properties,” *J. Mol. Liq.* (2016), 10.1016/j.molliq.2016.08.043.
- ³⁹C. S. Santos, H. V. R. Annapureddy, N. S. Murthy, H. K. Kashyap, E. W. Castner, Jr., and C. J. Margulis, “Temperature-dependent structure of methyltributylammonium bis(trifluoromethylsulfonyl)amide: X ray scattering and simulations,” *J. Chem. Phys.* **134**, 064501 (2011).
- ⁴⁰H. V. R. Annapureddy, H. K. Kashyap, P. M. De Biase, and C. J. Margulis, “What is the Origin of the Prepeak in the X-ray Scattering of Imidazolium-Based Room-Temperature Ionic Liquids?” *J. Phys. Chem. B* **114**, 16838–16846 (2010).
- ⁴¹H. K. Kashyap, C. S. Santos, H. V. R. Annapureddy, N. S. Murthy, C. J. Margulis, and E. W. Castner, Jr., “Temperature-Dependent Structure of Ionic Liquids: X-ray Scattering and Simulations,” *Faraday Discuss.* **154**, 133–143 (2012).
- ⁴²J. N. C. Lopes and A. A. H. Pádua, “Molecular Force Field for Ionic Liquids III: Imidazolium, Pyridinium, and Phosphonium Cations; Chloride, Bromide, and Dicyanamide Anions,” *J. Phys. Chem. B* **110**, 19586–19592 (2006).
- ⁴³A. Triolo, O. Russina, H.-J. Bleif, and E. Di Cola, “Nanoscale segregation in room temperature ionic liquids,” *J. Phys. Chem. B* **111**, 4641–4644 (2007).

- ⁴⁴H. K. Kashyap, C. S. Santos, R. P. Daly, J. J. Hettige, N. S. Murthy, H. Shirota, E. W. Castner, Jr., and C. J. Margulis, “How Does the Ionic Liquid Organizational Landscape Change when Nonpolar Cationic Alkyl Groups Are Replaced by Polar Isoelectronic Diethers?” *J. Phys. Chem. B* **117**, 1130–1135 (2013).
- ⁴⁵O. Russina, L. Gontrani, B. Fazio, D. Lombardo, A. Triolo, and R. Caminiti, “Selected chemical-physical properties and structural heterogeneities in 1-ethyl-3-methylimidazolium alkyl-sulfate room temperature ionic liquids,” *Chem. Phys. Lett.* **493**, 259–262 (2010).
- ⁴⁶M. Macchiagodena, F. Ramondo, A. Triolo, L. Gontrani, and R. Caminiti, “Liquid Structure of 1-Ethyl-3-methylimidazolium Alkyl Sulfates by X-ray Scattering and Molecular Dynamics,” *J. Phys. Chem. B* **116**, 13448–13458 (2012).
- ⁴⁷B. Wu, H. Shirota, and J. Edward W. Castner, “Structure of Ionic Liquids with Cationic Silicon-Substitutions,” *J. Chem. Phys.* **145** (2016), 10.1063/1.4962257.
- ⁴⁸T. L. Greaves, D. F. Kennedy, S. T. Mudie, and C. J. Drummond, “Diversity Observed in the Nanostructure of Protic Ionic Liquids,” *J. Phys. Chem. B* **114**, 10022–10031 (2010).
- ⁴⁹R. Hayes, S. Imberti, G. G. Warr, and R. Atkin, “Pronounced sponge-like nanostructure in propylammonium nitrate,” *Phys. Chem. Chem. Phys.* **13**, 13544–13551 (2011).
- ⁵⁰O. Russina, F. Lo Celso, M. Di Michiel, S. Passerini, G. B. Appetecchi, F. Castiglione, A. Mele, R. Caminiti, and A. Triolo, “Mesoscopic structural organization in triphilic room temperature ionic liquids,” *Faraday Discuss.* **167**, 499–513 (2013).
- ⁵¹K. Shimizu, A. A. Freitas, and J. N. C. Lopes, “Structural characterization of the [CnC1im][C4F9SO3] ionic liquid series: Alkyl versus perfluoroalkyl side chains,” *J. Mol. Liq.* (2016), 10.1016/j.molliq.2016.08.014.
- ⁵²T. A. Fadeeva, P. Husson, J. A. DeVine, M. F. Costa Gomes, S. G. Greenbaum, and E. W. Castner, Jr., “Interactions Between Water and 1-butyl-1-methylpyrrolidinium Ionic Liquids,” *J. Chem. Phys.* **143**, 064503 (2015).
- ⁵³M. Liang, S. Khatun, and E. W. Castner, Jr., “Communication: Unusual Structure and Transport in Ionic Liquid-Hexane Mixtures,” *J. Chem. Phys.* **142**, 121101 (2015).
- ⁵⁴A. Hammersley, S. Svensson, M. Hanfland, A. Fitch, and D. Hausermann, “Two-dimensional detector software: From real detector to idealised image or two-theta scan.” *High Pressure Res.* **14**, 235–248 (1996).

- ⁵⁵X. Qiu, J. W. Thompson, and S. J. L. Billinge, "PDFgetX2: a GUI-driven program to obtain the pair distribution function from X-ray powder diffraction data." *J. Appl. Cryst.* **37**, 678 (2004).
- ⁵⁶M. J. Abraham, T. Murtola, R. Schulz, S. Pll, J. C. Smith, B. Hess, and E. Lindahl, "GROMACS: High performance molecular simulations through multi-level parallelism from laptops to supercomputers," *SoftwareX* **1-2**, 19–25 (September 2015).
- ⁵⁷S. Pronk, S. Pall, R. Schulz, P. Larsson, P. Bjelkmar, R. Apostolov, M. R. Shirts, S. J. C., P. M. Kasson, D. van der Spoel, B. Hess, and E. Lindahl, "GROMACS 4.5: a high-throughput and highly parallel open source molecular simulation toolkit." *Bioinformatics* **29**, 845–854 (2013).
- ⁵⁸H. J. C. Berendsen, D. van der Spoel, and R. van Drunen, "GROMACS: A message-passing parallel molecular dynamics implementation." *Comp. Phys. Comm.* **91**, 43–56 (1995).
- ⁵⁹D. T. Cromer and J. B. Mann, "X-ray scattering factors computed from numerical Hartree-Fock wave functions," *Acta Cryst.* **A24**, 321–324 (1968).
- ⁶⁰E. Prince, ed., *International Tables for Crystallography : Volume C: Mathematical, Physical and Chemical Tables, Third Edition* (Kluwer Academic Publishers, 2004).
- ⁶¹E. Lorch, "Neutron Diffraction by Germania, Silica and Radiation-damaged Silica Glasses," *J. Phys. C: Solid State Phys.* **2**, 229–237 (1969).
- ⁶²J. Du, C. J. Benmore, R. Corrales, R. T. Hart, and J. K. R. Weber, "A molecular dynamics simulation interpretation of neutron and X-ray diffraction measurements on single phase Y_2O_3 - Al_2O_3 glasses," *J. Phys.: Condens. Matter* **21**, 205102 (2009).
- ⁶³N. W. Ashcroft and D. C. Langreth, "Structure of Binary Liquid Mixtures. I," *Phys. Rev.* **156**, 685–692 (1967).
- ⁶⁴J. L. Lebowitz, "Exact Solution of Generalized Percus-Yevick Equation for a Mixture of Hard Spheres," *Phys. Rev.* **133**, A895–A899 (1964).
- ⁶⁵R. C. Rizzo and W. L. Jorgensen, "OPLS All-Atom Model for Amines: Resolution of the Amine Hydration Problem," *J. Am. Chem Soc.* **121**, 4827–4836 (1999).
- ⁶⁶E. K. Watkins and W. L. Jorgensen, "Perfluoroalkanes: Conformational Analysis and Liquid-State Properties from ab Initio and Monte Carlo Calculations," *J. Phys. Chem. A* **105**, 4118–4125 (2001).

- ⁶⁷J. N. C. Lopes, J. Deschamps, and A. A. H. Pádua, "Modeling Ionic Liquids Using a Systematic All-Atom Force Field," *J. Phys. Chem. B* **108**, 2038–2047 (2004).
- ⁶⁸J. N. C. Lopes and A. A. H. Pádua, "Molecular Force Field for Ionic Liquids Composed of Triflate or Bistriflylimide Anions," *J. Phys. Chem. B* **108**, 16893–16898 (2004).
- ⁶⁹K. Shimizu, D. Almantariotis, M. F. C. Gomes, A. A. H. Pádua, and J. N. C. Lopes, "Molecular Force Field for Ionic Liquids V: Hydroxyethylimidazolium, Dimethoxy-2- Methylimidazolium, and Fluoroalkylimidazolium Cations and Bis(Fluorosulfonyl)Amide, Perfluoroalkanesulfonylamide, and Fluoroalkylfluorophosphate Anions," *J. Phys. Chem. B* **114**, 3592–3600 (2010).
- ⁷⁰J. N. C. Lopes and A. A. H. Pádua, "CL&P: A generic and systematic force field for ionic liquids modeling," *Theor Chem Acc* **131**, 1129 (2012).
- ⁷¹E. O. Stejskal, "Use of Spin Echoes in a Pulsed Magnetic Field Gradient to Study Anisotropic, Restricted Diffusion and Flow," *J. Chem. Phys.* **43**, 3597–3603 (1965).
- ⁷²J. E. Tanner, "Use of the Stimulated Echo in NMR Diffusion Studies," *J. Chem. Phys.* **52**, 2523 (1970).
- ⁷³D. Wu, A. Chen, and C. Johnson, "An Improved Diffusion-Ordered Spectroscopy Experiment Incorporating Bipolar-Gradient Pulses," *J. Magn. Reson.* **A115**, 260–264 (1995).
- ⁷⁴B. Antalek, *Concepts Magn. Reson.* **14**, 225–258 (2002).
- ⁷⁵T. Köddermann, D. Paschek, and R. Ludwig, "Molecular Dynamic Simulations of Ionic Liquids: A Reliable Description of Structure, Thermodynamics and Dynamics," *ChemPhysChem* **8**, 2464–2470 (2007).
- ⁷⁶J. N. Canongia Lopes, K. Shimizu, A. A. H. Pádua, Y. Umebayashi, S. Fukuda, K. Fujii, and S.-i. Ishiguro, "A Tale of Two Ions: The Conformational Landscapes of Bis(trifluoromethanesulfonyl)amide and N,N-Dialkylpyrrolidinium," *J. Phys. Chem. B* **112**, 1465–1472 (2008).
- ⁷⁷M. Brehm and B. Kirchner, "TRAVIS - A Free Analyzer and Visualizer for Monte Carlo and Molecular Dynamics Trajectories," *J. Chem. Inf. Model.* **51**, 2007–2023 (2011), TRAVIS Version 20160101.
- ⁷⁸W. Humphrey, A. Dalke, and K. Schulten, "VMD – Visual Molecular Dynamics," *J. Mol. Graph. Model.* **14**, 33–38 (1996).
- ⁷⁹P. A. Hunt, C. R. Ashworth, and R. P. Matthews, "Hydrogen bonding in ionic liquids," *Chemical Society Reviews* **44**, 1257–1288 (2015).

- ⁸⁰H. K. Kashyap, C. S. Santos, N. S. Murthy, J. J. Hettige, K. Kerr, S. Ramati, J. Gwon, M. Gohdo, S. I. Lall-Ramnarine, J. F. Wishart, C. J. Margulis, and E. W. Castner, Jr., "Structure of 1-Alkyl-1-methylpyrrolidinium Bis(trifluoromethylsulfonyl)amide Ionic Liquids with Linear, Branched, and Cyclic Alkyl Groups," *J. Phys. Chem. B* **117**, 15328–15337 (2013).
- ⁸¹C. S. Santos, N. S. Murthy, G. A. Baker, and E. W. Castner, Jr., "Communication: X-ray scattering from ionic liquids with pyrrolidinium cations," *J. Chem. Phys.* **134**, 121101 (2011).
- ⁸²A. Noda, K. Hayamizu, and M. Watanabe, "Pulsed-Gradient Spin-Echo ^1H and ^{19}F NMR Ionic Diffusion Coefficient, Viscosity, and Ionic Conductivity of Non-Chloroaluminate Room-Temperature Ionic Liquids," *J. Phys. Chem. B* **105**, 4603–4610 (2001).
- ⁸³H. Tokuda, K. Hayamizu, K. Ishii, M. A. B. H. Susan, and M. Watanabe, "Physicochemical Properties and Structures of Room Temperature Ionic Liquids. 1. Variation of Anionic Species," *J. Phys. Chem. B* **108**, 16593–16600 (2004).
- ⁸⁴H. Tokuda, K. Hayamizu, K. Ishii, M. A. B. H. Susan, and M. Watanabe, "Physicochemical Properties and Structures of Room Temperature Ionic Liquids. 2. Variation of Alkyl Chain Length in Imidazolium Cation," *J. Phys. Chem. B* **109**, 6103–6110 (2005).
- ⁸⁵H. Tokuda, K. Ishii, M. A. B. H. Susan, S. Tsuzuki, K. Hayamizu, and M. Watanabe, "Physicochemical Properties and Structures of Room-Temperature Ionic Liquids. 3. Variation of Cationic Structures," *J. Phys. Chem. B* **110**, 2833–2839 (2006).
- ⁸⁶H. Tokuda, S. Tsuzuki, M. A. B. H. Susan, K. Hayamizu, and M. Watanabe, "How Ionic Are Room-Temperature Ionic Liquids? An Indicator of the Physicochemical Properties," *J. Phys. Chem. B* **110**, 19593–19600 (2006).
- ⁸⁷K. R. Harris, "The fractional Stokes-Einstein equation: Application to Lennard-Jones, molecular, and ionic liquids," *J. Chem. Phys.* **131**, 054503 (2009).
- ⁸⁸A. Kaintz, G. Baker, A. Benesi, and M. Maroncelli, "Solute Diffusion in Ionic Liquids, NMR Measurements and Comparisons to Conventional Solvents," *J. Phys. Chem.* **117**, 11697–11708 (2013).
- ⁸⁹F. Castiglione, M. Moreno, G. Raos, A. Famulari, A. Mele, G. B. Appetecchi, and S. Passerini, "Structural Organization and Transport Properties of Novel Pyrrolidinium-Based Ionic Liquids with Perfluoroalkyl Sulfonylimide Anions," *J. Phys. Chem. B* **113**, 10750–10759 (2009).

- ⁹⁰J. Reiter, S. Jeremias, E. Paillard, M. Winter, and S. Passerini, “Fluorosulfonyl-(trifluoromethanesulfonyl)imide ionic liquids with enhanced asymmetry,” *Phys. Chem. Chem. Phys.* **15**, 2565–2571 (2013).
- ⁹¹J. C. Araque, J. J. Hettige, and C. J. Margulis, “Modern Room Temperature Ionic Liquids, a Simple Guide to Understanding Their Structure and How It May Relate to Dynamics,” *J. Phys. Chem. B* **119**(4), 12727–12740 (2015).
- ⁹²T. Yan, C. J. Burnham, M. G. D. Pópolo, and G. A. Voth, “Molecular Dynamics Simulation of Ionic Liquids: The Effect of Electronic Polarizability,” *J. Phys. Chem. B* **108**, 11877–11881 (2004).
- ⁹³T. Yan, S. Li, W. Jiang, X. Gao, B. Xiang, and G. A. Voth, “Structure of the Liquid-Vacuum Interface of Room-Temperature Ionic Liquids: A Molecular Dynamics Study,” *J. Phys. Chem. B* **110**, 1800–1806 (2006).
- ⁹⁴O. Borodin, “Polarizable Force Field Development and Molecular Dynamics Simulations of Ionic Liquids,” *J. Phys. Chem. B* **113**, 11463–11478 (2009).
- ⁹⁵D. Bedrov and O. Borodin, “Thermodynamic, Dynamic, and Structural Properties of Ionic Liquids Comprised of 1-Butyl-3-methylimidazolium Cation and Nitrate, Azide, or Dicyanamide Anions,” *J. Phys. Chem. B* **114**, 12802–12810 (2010).
- ⁹⁶V. Lesch, Z. Li, D. Bedrov, O. Borodin, and A. Heuer, “The influence of cations on lithium ion coordination and transport in ionic liquid electrolytes: a MD simulation study,” *Phys. Chem. Chem. Phys.* **18**, 382–392 (2016).
- ⁹⁷T. I. Morrow and E. J. Maginn, “Molecular Dynamics Study of the Ionic Liquid 1-n-Butyl-3-methylimidazolium Hexafluorophosphate,” *J. Phys. Chem. B* **106**, 12807–12813 (2002).
- ⁹⁸H. Liu and E. Maginn, “A molecular dynamics investigation of the structural and dynamic properties of the ionic liquid 1-n-butyl-3-methylimidazolium bis(trifluoromethanesulfonyl)imide,” *J. Chem. Phys.* **135**, 124507 (2011).
- ⁹⁹E. D. Hazelbaker, S. Budhathoki, A. Katihar, J. K. Shah, E. J. Maginn, and S. Vasenkov, “Combined Application of High-Field Diffusion NMR and Molecular Dynamics Simulations To Study Dynamics in a Mixture of Carbon Dioxide and an Imidazolium-Based Ionic Liquid,” *J. Phys. Chem. B* **116**, 9141–9151 (2012).
- ¹⁰⁰V. V. Chaban and I. V. Voroshylova, “Systematic Refinement of Canonical Lopes – Pádua Force Field for Pyrrolidinium-Based Ionic Liquids,”

- J. Phys. Chem. B **119**, 6242–6249 (2015).
- ¹⁰¹Y. Yao, Y. Kanai, and M. L. Berkowitz, “Role of Charge Transfer in Water Diffusivity in Aqueous Ionic Solutions,” J. Phys. Chem. Lett. **5**, 2711–2716 (2014).
- ¹⁰²S. Nosé, “A unified formulation of the constant temperature molecular dynamics methods.” J. Chem. Phys. **81**, 511–519 (1984).
- ¹⁰³S. Nosé, “A molecular dynamics method for simulations in the canonical ensemble.” Mol. Phys. **52**, 255–268 (1984).
- ¹⁰⁴M. Parrinello and A. Rahman, “Polymorphic transitions in single crystals: A new molecular dynamics method.” J. Appl. Phys. **52**, 7182–7190 (1981).